Sharwes Scientific Journal (SSJ)
Volume 6, Issue 1, 2025, pp 146-163, ISSN 3079-6040

Comparative Effect of Indium, Molybdenum, and Strontium Doping on Structural, Vibrational, and Optical Properties of ZnO Sprayed Thin Films

Ramadan Ebrahim Shaiboub [1*], Majda Mokhtari [2], Nacer Boucherou [3], Aicha Ziouche [3], Abdelwaheb Boukhachem [4,5], Mosbah Amlouk [5]

[1]Physics Department, Faculty of Education, Nalut University, Nalut, Libya.
[2]University of Larbi Ben M'Hidi, Algeria.
[3]Research Center in Industrial Technologies (CRTI), Algeria.
[4]Nanomaterials and Systems for Renewable Energies Laboratory, Energy Research and Technology Center, Technopole Borj Cedria, Tunisia.
[5]Nanomaterials, Nanotechnologies, and Energy Laboratory, University of Tunis Al Manar, Tunisia.

* Corresponding Author: Ramadan Shaiboub | r.shaiboub@nu.edu.ly

Received: 17-04-2025 | Accepted: 21-04-2025 | Available online: 27-04-2025 | DOI:10.26629/ssj.2025.08

ABSTRACT

Zinc oxide (ZnO) thin films were deposited on glass substrates using a simple microspray technique, and some of the resulting films were doped with strontium, indium, and molybdenum at molar concentrations of 1%. In addition to classical structural studies, such as X-ray diffraction (XRD) patterns, which revealed peaks corresponding to hexagonal zinc oxide wurtzite, topographical observations using atomic electron microscopy (AFM), and vibrational properties using Raman spectroscopy with excitation wavelengths at 488 nm where the FWHM value for Raman spectroscopy was approximately 15 cm-1, comprehensive optical measurements were also performed using photothermal techniques. The dispersion properties of the differently doped layers were derived from their transmittance and reflectance spectra over an extended wavelength range. The Raman shift E1(LO) mode was found to decrease with the oxidation number of the doping elements. The shift was found to be a positive factor with peaks almost the same in energy as the Urbach energy. Finally, the analysis of the refractive index using the Urbach-Martinsen model allowed for the nanoscale explanations for the variation in the doping-related evolution of the Urbach tails. The Urbach coefficients were calculated, and the results showed that the photothermal expansion decreases with increasing oxidation number of the doped elements. The optical properties of the refractive index were also calculated, and it was also observed that it decreases with wave length.

Keywords: Thin films, X-ray diffraction, Optical properties and Raman spectroscopy.

مقارنة تأثير تشويب الإنديوم و الموليبدينوم و السترونشيوم على الخواص التركيبية والاهتزازية والبصرية لأغشية أكسيد الزنك الرقيقة المرشوشة

رمضان شيبوب[1]، ماجدة مختاري[2]، ناصر بوشروي[3]، عائشة زيوشي[3]، عبد الوهاب بوخشم[4،5]، ومصباح أملوق[5]

1 قسم الفيزياء، كلية التربية، جامعة نالوت، نالوت، ليبيا

2 جامعة العربي بن مهيدي، الجزائر

3 مركز البحوث التقنيات الصناعية (CRTI)، الجزائر

4 مختبر المواد النانوية وأنظمة الطاقات المتجددة (LANSER)، مركز البحوث وتقنيات تكنولوجيا الطاقة في برج السدرية، تونس
5 مختبر المواد النانوية، تكنولوجيات النانو والطاقة، جامعة تونس المنار، تونس
*المؤلف المراسل: رمضان شيبوب | r.shaiboub@nu.edu.ly

استقبلت: 17-04-2025م | قبلت: 21-04-2025م | متوفرة على الانترنت | 27-04-2025م | DOI:10.26629/ssj.2025.08

ملخص البحث

رُسِّبت أغشية رقيقة من أكسيد الزنك (ZnO) على ركائز زجاجية باستخدام تقنية رش مجهري بسيطة، وشُوِّبَت بعض الأغشية الناتجة بالسترونشيوم والإنديوم والموليبدينوم بتركيزات مولية قدرها 1% بالإضافة إلى الدراسات البنيوية الكلاسيكية، مثل أنماط حيود الأشعة السينية (XRD)، التي كشفت عن قمم تُقابل (وورتزيت) لاكسيد الزنك السداسي، والملاحظات الطبوغرافية باستخدام المجهر الإلكتروني الذري (AFM)، وخصائص الاهتزاز باستخدام مطيافية رامان مع أطوال موجية للإثارة عند 488 نانومتر، حيث بلغت قيمة عرض الذروة عند الطرف الأقصى (FWHM) لمطيافية رامان حوالي 15 سم$^{-1}$، أُجريت قياسات بصرية شاملة باستخدام التقنيات الضوئية الحرارية. استُنبطت خصائص التشتت للطبقات المُشَوَّبة بشكل مختلف من أطياف نفاذيتها وانعكاسيتها على مدى أطوال موجية ممتدة. وُجِد أن نمط إزاحة رامان E1(LO) يتناقص مع عدد أكسدة العناصر المُشَوَّبة, ووجد أن هذا الانزياح عامل إيجابي، حيث تقاربت ذروات الطاقة فيه طاقة أورباخ. وأخيرًا، سمح تحليل معامل الانكسار باستخدام نموذج أورباخ – مارتنسن بتفسير التباين في تطور ذيول أورباخ المرتبط بالتشويب على المستوى النانوي. حُسبت معاملات أورباخ، وأظهرت النتائج أن التمدد الضوئي الحراري يتناقص مع زيادة رقم أكسدة العناصر المشوبة, كما حُسبت الخصائص البصرية لمعامل الانكسار ولوحظ أيضًا أنه يتناقص مع زيادة الطول الموجي.

الكلمات المفتاحية: الأغشية الرقيقة، حيود الأشعة السينية، الخصائص البصرية، ومطيافية رامان.

1. Introduction

Transparent conducting oxides (TCOs) material such as tin oxides and indium-doped oxide systems have been used in several devices, such as gas sensors, panel displays[1,2] and photovoltaic solar cells (PVCs). Among these oxides, zinc oxide has attracted considerable attention from those interested in the application to devices working in ultraviolet regions, with the interest specially lying in its wide bandgap, quantum confinement effects in accessible size ranges, and its attractive exciton binding energy (≈60 meV).[1,2] It has been recorded that zinc oxide is a hexagonal wurtzite structured semiconductor with high piezoelectric and gas-detecting properties.[1-6] Its deposition on glass-like substrates has been widely experimented and applied.[7-11] On the other hand, many doping elements for ZnO have been tried.[12-15] In some studies, the merits of indium and aluminum as effective doping agents have been pointed out.[16-19] ZnO thin film is deposited by different techniques which include pulsed laser deposition, sol-gel dip coting, magnetron sputtering, atomic layer deposition (ALD), and chemical vapor

deposition and spray pyrolysis techniques.[20-25] The spray pyrolysis deposition technique is a simple and relatively cost effective one. This work seeks the explanations to the effects of strontium, indium and molybdenum doping on ZnO sprayed thin films prepared in the same conditions in terms of structural, optical and morphological properties.

Experimental details

2.1. Undoped ZnO films preparation

ZnO thin films have been first prepared at a glass substrate temperature of 460°C using propanol and zinc acetate Zn $(CH_3CO_2)_2$: 10^{-2} M according to the chemical protocol summarized elsewhere.[20,21] The precursor mixture was acidified using acetic acid (pH = 5) and the carrier gas was nitrogen (pressure ≈0.35 bar) through a 0.5 mm diameter nozzle. Based on the optimization's work reported by Boubaker *et al*.[28] the distance between nozzle and substrates plane was fixed at 27 cm. In these thin films preparation, the flow rate of the mixture solutions was fixed at 4 ml/min throughout the deposition process. Finally, in order to avoid the effect of rapid cooling and its effects on crystal structure destruction, the coated substrates were allowed to cool down naturally to room temperature.

2.2 Strontium/ Indium/ Molybdenum doping

Under similar experimental conditions, strontium/indium/ molybdenum-doped ZnO thin films solutions have been fabricated by adding hydrated indium chloride ($InCl_3$, xH_2O, 99.9% purity) for indium doping, strontium chloride ($SrCl_2$, $2H_2O$, 99.9% purity) for strontium doping and Ammonium molybdate tetra-hydrated [$(NH_4)_6Mo_7O_{24}.4H_2O$ ACROS pure more than 99.0%] for Molybdenum doping to the precursor solution while maintaining acidity level. In the three elaborated samples, the strontium-to-zinc molar ratios [M]/[Zn] were taken all metal doping 0.01.

2.3 Characterizations techniques

The prepared films ZnO: Sr were investigated using X-ray diffractometry by means of a (*Philips PW1729 system*) using Cukα monochromatic radiation (λ=1.54059 Å) system. Surface topography of all obtained films was performed in contact mode by means of an atomic force microscopy (VEECO digital instrument). Raman spectroscopy was carried out by using Jobin Yvon HR Lab RAM in backscattering co-focal configuration at room temperature with a spatial resolution of 1 μm and spectral resolution less than 0.35 cm^{-1}. The light excitation is an Ar+ laser at the wavelength of 488 nm. The laser power was controlled at 8.5 mW on the sample surface. The laser beam on the surface was focused using 100 × objective lens. Optical transmittance T(λ) and reflectance R(λ) were monitored using a Schimadzu UV 3100 double-beam spectrophotometer, over a range of wavelengths (300-2000 nm) at room temperature.

3. Results and discussion

3.1. Structural properties

Figure 1 shows the XRD pattern of zinc oxide thin film prepared at 460°C. This spectrum depicts the presence of (001), (002), (101), (102) and (103), peaks corresponding to ZnO hexagonal würtzite (JCPDS No.: 036-1451 card). From this X-ray analysis, it is obvious that the crystallites have preferential orientation along (002). To obtain more information regarding

the structural quality of prepared ZnO sprayed thin film, some structural calculations have been made:

The interplanar spacing d_{hkl} of given Miller indices (h k l) values of Zn thin films were calculated by using Bragg equation[29-32]:

$$2d_{hkl}\sin\theta = n\lambda \quad (1)$$

Where n is the order of diffraction (usually n = 1) and λ is the X-ray wavelength. The lattices parameters, in fact, in the hexagonal structure, the plane spacing are related to the lattice constant a, b and c and the Miller indices by the following relation:

$$\frac{1}{d_{hkl}^2} = \frac{4}{3}\left(\frac{h^2+hk+k^2}{a^2}\right) + \frac{l^2}{c^2} \quad (2)$$

The calculated values of lattice parameters are given in table1. These values are in good agreement has been found between our results obtained and those reported elsewhere.[33-37]

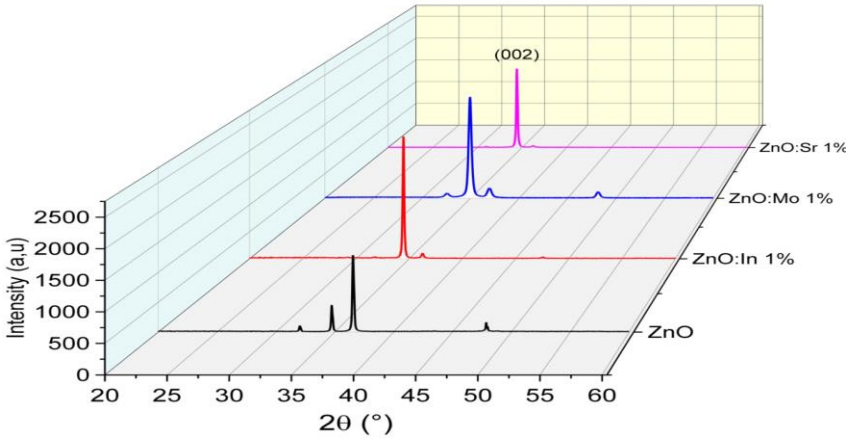

Fig. 1:X-ray diffraction spectra of Sr/In/Mo doped ZnO sprayed thin films

Table 1: Lattice parameters of ZnO:M thin film (M= Sr or In or Mo).

	a (Å)	c (Å)	Volume (Å³)	c/a
ZnO	3.2611	5.2276	48.1444	1.6030
ZnO :In 1%	3.2578	5.1992	47.7878	1.5959
ZnO :Mo 1%	3.2244	5.1345	46.2289	1.5924
ZnO :Sr 1%	3.2474	5.2040	47.9776	1.6017

At first glance, it can be seen that lattice parameters are strongly depended to metal doping. This is probably related to the difference in ionic radius of zinc and metal elements.[38] Also, the volume unit cell decreases with the oxidation number of the doping element (Sr^{+II}, In^{+III}, Mo^{+VI}). This property can affect the optical and opto-thermal properties of these doped ZnO prepared thin film. Indeed, this metal doping effect in terms in its cell's variation changes the compactness of ZnO compound and therefore inters-ionic interactions which can increases the structural stresses in these doped thin films with oxidation number of doping elements.

Moreover, based on peak intensities, it is found that the guidelines are not equal this leads us to study these guidelines through the texture coefficient (TC) which indicates the maximum preferred orientation through the most likely plan. TC (*h k l*) values have been calculated from X-ray data, using the following formula:

$$TC_{(hkl)} = \frac{I(hkl)/I_0(hkl)}{N^{-1}\sum I(hkl)/I_0(hkl)} \quad (3)$$

Where *I*(*hkl*) is the measured relative intensity of (*h k l*) plane, I_o (h k l) is the standard intensity of the same plane taken from the JCPDS data and *N* is the reflection number. Table 2 summarizes the calculated values of TC_{hkl} of ZnO: Sr spray thin film.

Table 2: TC of ZnO doped thin film.

	$TC_{(100)}$	**$TC_{(002)}$**	**$TC_{(101)}$**	**$TC_{(102)}$**	**$TC_{(103)}$**
ZnO	0.07	4.57	0.28	0.04	0.05
ZnO :In 1%	0.02	4.74	0.19	0.04	-
ZnO :Mo 1%	0.22	4.02	0.42	0.35	-
ZnO :Sr 1%	0.23	3.88	0.46	0.17	0.26

For all the films $TC_{(002)}$ is so high (>1) indicate that all films have a preferential growth with the c-axis perpendicular to the film plan. As (002) is the preferred orientation, some structural parameters such as crystallites size, stress and dislocation density were calculated related to this direction using the following relations[38-41]:

$$\begin{cases} D = \dfrac{k.\lambda}{\beta_{\frac{1}{2}}\cos(\theta)} & (4) \\ \xi = \dfrac{\beta_{\frac{1}{2}}}{4\tan(\theta)} & (5) \\ \delta = \dfrac{1}{D^2} & (6) \end{cases}$$

Where *k* =0.90, λ=1.54 Å is the wavelength of CuKα radiation, β is the XRD (002) pic's width at half maximum and θ is the Bragg's diffraction angle. Values of these structural parameters are listed in table3.

Table 3: Average values of Grain size, dislocation density and microstrain related to (002) orientation.

	$D_{(002)}$ (nm)	$\varepsilon_{(002)}$ (10^{-4})	$\delta_{(002)}$ (10^{14}lines/m^2)
ZnO	168.97	6.96	0.35
ZnO :In 1%	105.69	11.07	0.89
ZnO :Mo 1%	52.89	21.84	3.57
ZnO :Sr 1%	120.71	9.71	0.69

This structural calculation reveals that this binary oxide displays some flaws such as dislocations and strain. These defaults seem to be the result related to an additional mechanism which occurs during the formation of the thin film leading to the difference between the ionic radius of zinc and doping elements. This result is so required for possibly gas sensors device and open the way to interesting environmental applications. On the other hand, values of these structural parameters confirm the oxidation number variation. Indeed, the crystallite size decreases with oxidation number contrary to both stress and dislocation density which increase with oxidation number.

3.2. Properties of thin films

3.2.1 Raman analyses

In the structural study, several important issues have been clarified such as the crystal structure, the lattice parameters and structural defects. To reinforce this study, Raman spectroscopy is considered a sensitive tool for further investigation of the structure of matter. It is known in its wurtzite ZnO structure which belongs to the space group C6v 4 contains two Zn-O molecular units. Due to the number of n = 4 atoms in the unit cell, the number of phonons amounts to 3n = 12, leading to 3 acoustic modes; one longitudinal and two transversal modes (1xLA, 2xTA) and 3n - 3 = 9 optical phonons.[43] At the center of the Brilliance zone (Γ point) group theory predicts the irreducible representation of the optical phonons is given by la following relation[44,45]:

$$\Gamma = 1A_1+2B_1+1E_1+2E_2 \quad (7)$$

Where A_1 and E_1 are polar modes and are both infrared and Raman active, while E_2 modes are nonpolar and only Raman active. The nonpolar E_2 modes have two wave numbers, namely, E_2 (high) and E_2 (low) linked to the movement of both oxygen and Zn sub lattice. Strong E2 (high) mode is characteristic of the wurtzite lattice and indicates good crystallinity. The vibrations of A_1 and E_1 modes can polarize in unit cell, which creates a long-range electrostatic field splitting the polar modes into longitudinal optical (LO) and transverse optical (TO) component. The E_1 (LO) mode is related to the presence of oxygen vacancies, and interstitial Zn as well as their complexes. The B_1 modes are Raman and infrared inactive (silent modes).

In this work, the effect of doping element incorporation in ZnO in terms of vibrational properties was performed through the Raman spectrum using 488 nm wavelengths excitation (visible range). Figure 2 shows Raman spectra of In/Mo/Sr doped ZnO sprayed thin films. At first glance, we note the sharpness of the peaks corresponding to zinc oxide and their intensities attests a good crystallization of these prepared thin films. On the other hand, and it was found in this investigation that the FWHM of Raman spectroscopy has a small value (around 15cm$^-$

[1]); this indicates that the prepared thin film has a high crystalline quality which is consistent with the results of the XRD described above.

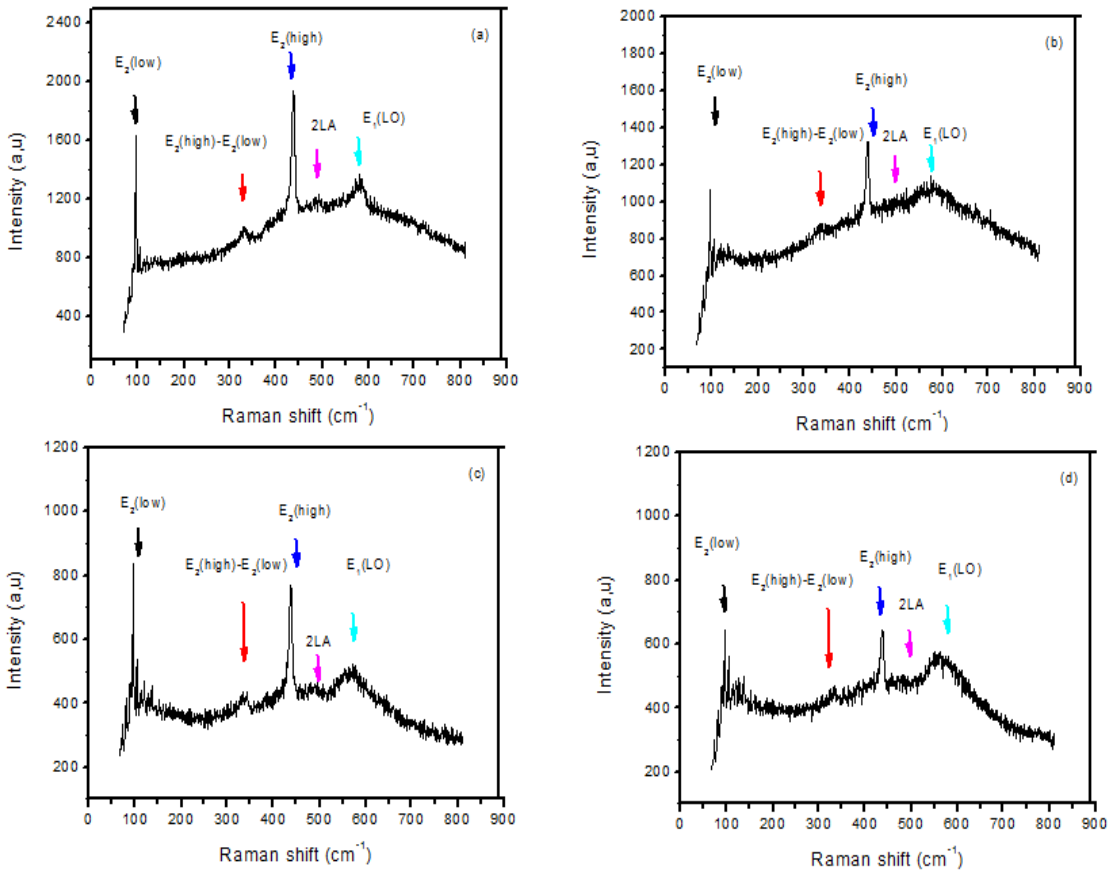

Fig. 2: Raman spectra of Sr/In/Mo doped-ZnO thin films using 488 nm excitation.

By examining the Raman spectra of different prepared thin films, it is noted that the mode E_2 (high) located around 440 cm^{-1} continues as a main mod of these ZnO doped thin films. The positions of other peaks of the Raman spectrum and their corresponding modes are summarized in table 4.

Table 4: Raman shift of the observed mode in ZnO sprayed thin film.

	ZnO	ZnO:Sr 1%	ZnO:In 1%	ZnO:Mo 1%
E_2(low) (cm^{-1})	96	96	96	96
E_2(high)- E_2(low) (cm^{-1})	329	331	341	333
E_2(high) (cm^{-1})	438	438	438	437
2LA (cm^{-1})	493	485	481	483
E_1(LO) (cm^{-1})	581	576	572	564

It is found that the Raman shift related to E_1(LO) mode decreases with oxidation number of the doping elements. Also, it is observed that the FWHM of the main mode increases with the oxidation number (Table5). This indicates that the presence of some defaults which increase

the oxidation number. This result is consistent with the results mentioned in the structural section indeed, the dislocation density related to molybdenum doping is high than other.

Table 5: Full width at half maximum of E1(LO) main mode of ZnO doped films.

	ZnO	ZnO:Sr 1%	ZnO:In 1%	ZnO:Mo 1%
FWHM of E_2(high) (cm^{-1})	18	20	22	24

3.3. Atomic force microscopy (AFM) observations

To reinforce XRD analysis, AFM observations have been performed, figure 3 shows 3D AFM micrographs of theses ZnO sprayed thin films. Based on these observations, it is found that the films are homogeneous. This property offers the possibility to use these ZnO: M (M= Sr, In or Mo) films as optical material.

The root means square roughness (Rq) which is considered as the average of square deviation from the mean line within the assessment length L using the following relation[29]:

$$R_q = \sqrt{\frac{1}{L}\int_0^L (z - z_m)^2 dx} \qquad (8)$$

Rq values are gathered in table 6

Table 6: Roughness values of Sr/In/Mo doped-ZnO prepared thin film.

	Zno	ZnO :Sr	Zno :In	ZnO :Mo
Rq(nm)	32	28	90	20

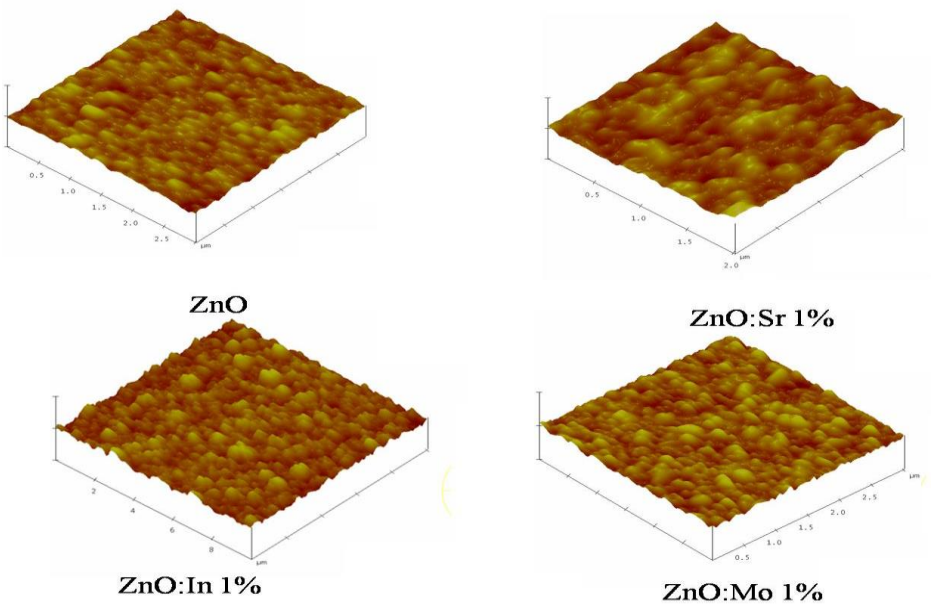

Fig. 3:AFM images of the undoped and Sr/In/Mo-doped ZnO.

It is found that roughness varies in a random manner with the oxidation number this is probably governed by the difference in ionic radius.

3.4. Optical properties

3.4.1 Reflectance and transmittance spectra

The optical transmission T□□) and reflectance R(□) spectra of ZnO:Sr/In/Mo films in the wavelength range 250-2000 nm (covering the UV-visible-near IR range) are shown in figure 4 (a)-(b). It can be seen the absence of interference fringes. These spectra show that in the visible range, the prepared films exhibit low reflectance (less than 20%) and high transparency (around 80%). In addition, an interference phenomenon was also observed, which indicates a smooth surface for all prepared films.

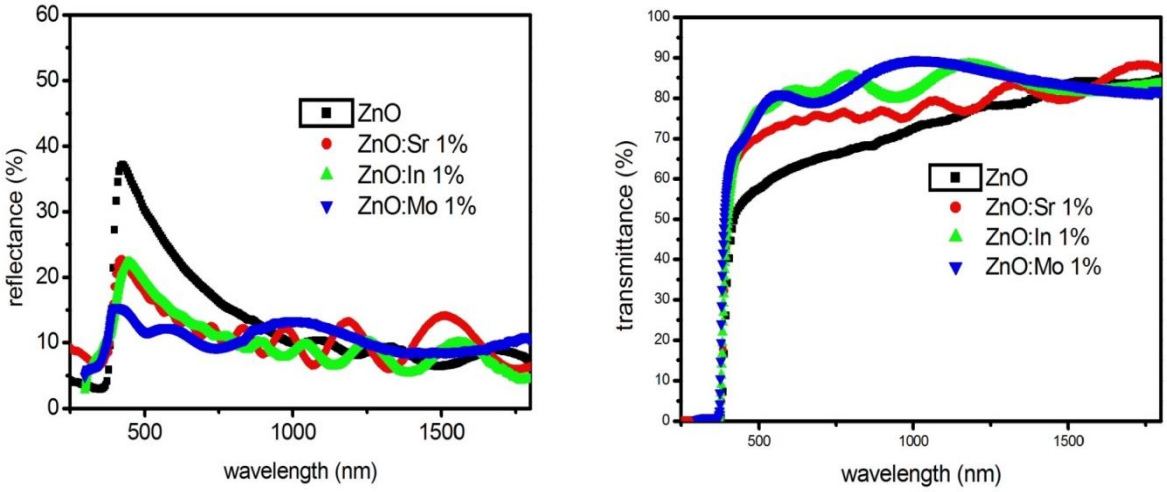

Fig. 4: Reflectance and transmittance spectra.

3-4-2. Band gap energy calculation

The absorption coefficient of ZnO thin films was determined from transmittance and reflectance measurements using the following expression[47-50]:

$$\alpha = \frac{1}{e} Ln(\frac{(1-R)^2}{T}) \qquad (9)$$

Where e is the layer thickness. The value of band gap is estimated from fundamental absorption edge of the films. The optical band gap of the ZnO films was calculated from the relationship between the optical absorption coefficient and the transmittance by using the Tauc model. For a semiconductor with a direct band gap, the optical band gap can be expressed by using the Taucrelation:

$$\alpha h\nu = A(h\upsilon - E_g)^{\frac{1}{2}} \qquad (10)$$

Where A is proportionality constant, hν is the photon energy of the incident light and E_g is the optical band gap. The optical band gap was obtained by extrapolating the tangential line to the photon energy axis in the plot of $(\alpha h\nu)^2$ versus hν, which is shown in figure 5. The calculated values of optical band gap are gathered in table 7.

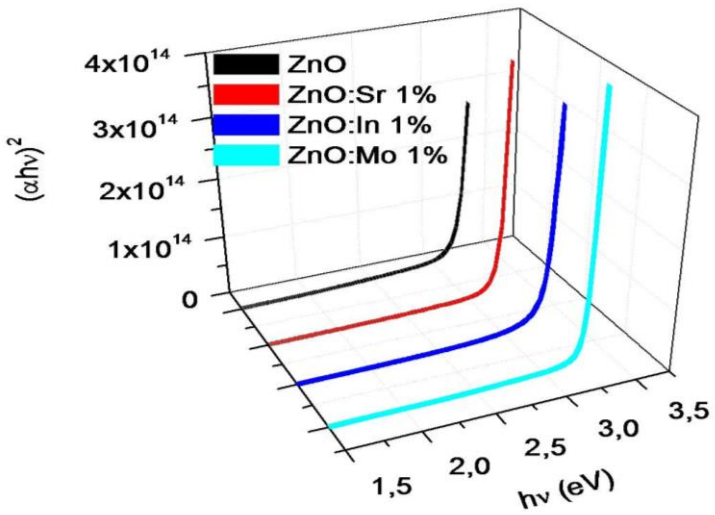

Fig. 5: Plot of $(\alpha h\nu)^2$ vs photon energy.

Table 7: The band gap value of Sr/In/Mo doped-ZnO prepared thin film.

	Eg (eV)
ZnO	3.219
ZnO :Sr 1%	3.255
ZnO :In1%	3.258
ZnO :Mo1%	3.281

In correlation with the AFM observation, it is found strongly influenced of surface morphology on the optical transmittance of ZnO doped thin film. Especially, the absorption wavelength has the same variation of the roughness of the prepared films. This absorbance wavelength of the ZnO thin films can calculate from the first derivative of the transmittance with respect to wavelength. Indeed, the absorption wavelength corresponds to the peak of $\frac{dT}{d\lambda}$.

Figure 6, shows the first derivative curves of transmittance vs wavelength. The energy related to this absorption's wavelengths corresponds to the optical band gap. Indeed, the attribution of the different peaks of the derivative of transmittance spectra (Figure 6) to optical band gap was trivial and experimentally proved. Nevertheless, the recorded shift in ZnO:Sr, Zno:In, ZnO:Mo spectra (taking ZnO spectrum as reference) remained hardly explicable. In the actual study, the shift, for each doping agent was found to have sensibly the same values, in term of energy, of Urbach energy. Table 8 summarizes the absorption wavelength of ZnO doped films.

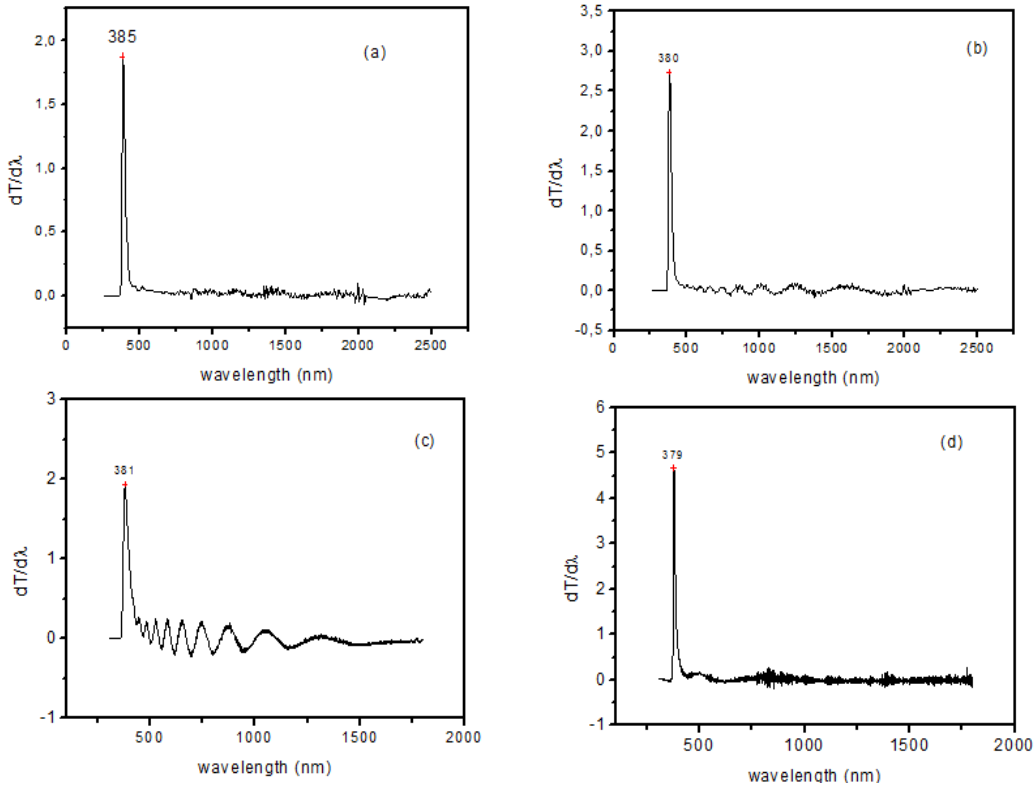

Fig. 6: Variation dT/dλ with wavelength.

Table 8: Calculated values of absorption wavelength.

	ZnO	ZnO :Sr	ZnO :In	ZnO :Mo
Absorption wavelength (nm)	385	380	381	379

Also, Figure 7 shows the variation of both roughness and absorption wavelength with oxidation number.

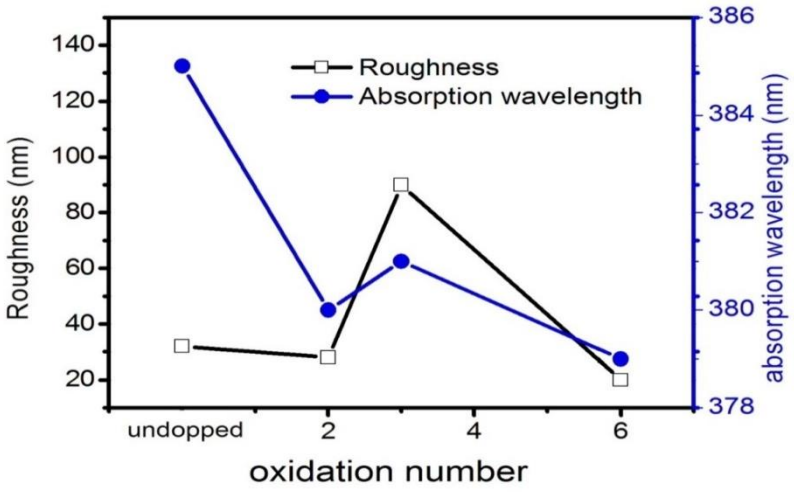

Fig. 7: variation of roughness and wavelength absorption oxidation number of doping.

On the other hand, the Urbach energy (E_U) is used to characterize the disorder degree the prepared thin films. The width of the band tails associated with valance and conduction bands was believed to be originated from electron transition between localized states, where the density of these localized states is exponentially dependent on energy.[51] The relation is given by empirical Urbach rule: The relation can be rewritten as tells us about defect concentration as materials with large Urbach energy would have a greater tendency to convert weak bonds into defects. Its values were determined from the slope of the linear region of the curves Ln(α) vs. hυ as shown in figure 8.

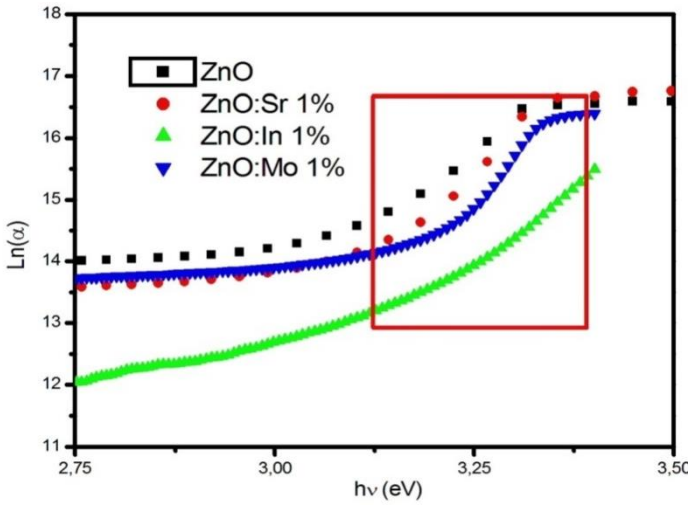

Fig. 8: Plot of Ln(α) versus hν.

The values of E_U are also listed in table 9. It is found that these values are in the range of 66 to 120 meV. As reported by Davis and Mott,[52] Urbach effect corresponds to amorphous semiconductors as reported, the less values of Urbach energy indicates a good crystallinity of these prepared thin films.[53] This result is in good agreement with the structural study.

Table 9: The Urbach energy value of Sr/In/Mo doped-ZnO prepared thin film.

	EU (meV)
ZnO	120.24
ZnO :Sr 1%	84.01
ZnO :In1%	119.68
ZnO :Mo1%	66.15

3. 4. 3. Opto-thermal investigation

Opto-thermal properties of ZnO doped thin films were investigated through the The Amlouk–Boubaker opto-thermal expansivity Ψ_{AB}.[54-58] This parameter has been defined by:

$$\Psi_{AB} = \frac{D}{\hat{\alpha}} \qquad (11)$$

Where D is the thermal diffusivity and $\hat{\alpha}$ is the effective absorptivity which is defined as the mean normalized absorbance weightedby the spectral solar standard irradiance $(I(\lambda)_{AM1.5})$.

$$\hat{\alpha} = \frac{\int_{\lambda_{min}}^{\lambda\,max} I(\lambda)_{AM1.5} \times \alpha(\lambda) d\lambda}{\int_{\lambda_{min}}^{\lambda\,max} I(\lambda)_{AM1.5} d} \qquad (12)$$

Where λ_{min} and λ_{max} are the limit of the visible spectrum and where: $I(\lambda)_{AM1.5}$ is the Reference Solar Spectral Irradiance. Table 10, summarizes the calculated values of Ψ_{AB} of ZnO doped films.

Table 10: Opto-thermal expansivity Ψ_{AB} values.

sample	ZnO	ZnO:Sr 1%	ZnO:In 1%	ZnO:Mo 1 %
Ψ_{AB} (10^{-12} m^3 s^{-1})	19.70	23.68	14.5	6.43

From these calculated values of opto-thermal expansively, it can be seen that Ψ_{AB} value deceases with oxidation number of doping elements. This phenomenon is probably related to the increases of free carrier with oxidation number and therefore the increasing of the absorptivity.

3.4.4. Refractive index and extinction coefficient.

The optical characteristics of dispersion refractive index $n(\lambda)$ and extinction coefficient $k(\lambda)$ have been calculated using optical experimental measurements. Given the existence of interference phenomena in the transmission and reflection spectra, this calculation is based on the study of the total transmission as well as the total reflection, which result from the interference of the various light rays transmitted and reflected at the air/sample and sample/substrate interfaces according to the method proposed by Belgacem *et al*.[59] and Bathe *et al*.[60] by solving the nonlinear system.

$$\begin{cases} f_1(n,k,\lambda) = R - R_{exp} = 0 & (13) \\ f_2(n,k,\lambda) = T - T_{exp} = 0 & (14) \end{cases}$$

The plots of $n(\lambda)$ and $k(\lambda)$ are presented respectively in figures 9, 10. It is observed that the extinction coefficient decreases abruptly with the wavelength. Their low values were obtained in visible range which is consistent with the transparency of prepared films. Likewise, the refractive index decreases hyperbolically with the wavelength; this variation can be modeled by Cauchy law[61-63]:

$$n = A + \frac{B}{\lambda^2} \qquad (15)$$

Where A and B are the Cauchy's parameters and λ is the wavelength. This implies that the films have normal dispersion along the entire studied range of wavelength. Cauchy parameters values are gathered in table 11. Also, this hyperbolic variation was used to study the optical dispersion parameters E_0 and E_d, derived from the real part of the final refractive index are evaluated according to single effective oscillator model proposed by Wemple and Di-Domenico.[64]

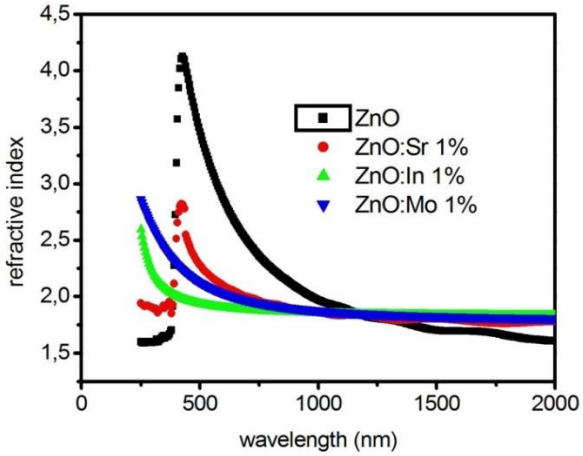

Fig. 9: Refractive index variations of refractive index with wavelength.

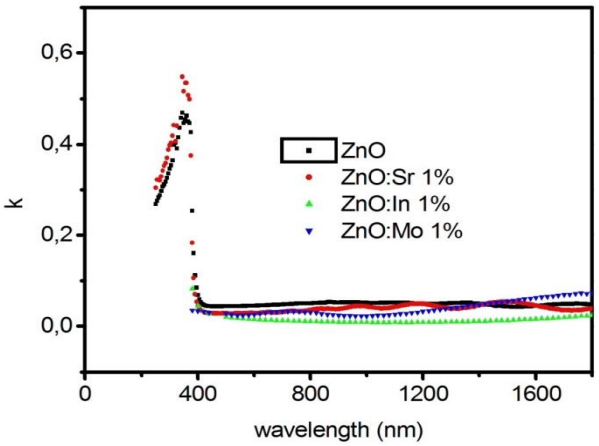

Fig. 10: extinction coefficient variations with wavelength.

Table 11: Values of Cauchy and Wemple and Di-Dominico parameters of Sr/In/Mo doped-ZnO prepared thin film.

	A	B (μm^2)	E_0 (eV)	E_d (eV)
ZnO	1.48	0.119	3.85	8.825
ZnO :Sr 1%	1.72	0.138	3.65	8.300
ZnO :In 1%	1.80	0.031	6.10	13.91
ZnO :Mo 1%	1.78	0.087	3.98	9.085

It is well known from the dispersion theory that in the region of low absorption, the refractive index is given in a single- oscillator model by the expression:

$$n^2 = 1 + \frac{E_0 E_d}{E_0^2 - E^2} \qquad (16)$$

Where E=hν is the incident photon energy, E_0 is the single-oscillator energy and E_d is the dispersion energy. From refractive index, E_0 and E_d values which listed in table 11. It is found that values of both A and B depend on Sr doping furthermore; the dispersive energy (E_d) has a maximum around 15 eV for 6% doping level. This result confirms the particularity of this doing level. Finally, interaction of the doped layers with electromagnetic radiation has been modeled through complex dielectric constant $\varepsilon(\lambda)$ defined by:

$$\varepsilon(\lambda) = (n(\lambda) + ik(\lambda))^2 = \varepsilon 1(\lambda) + i\varepsilon 2(\lambda) \qquad (17)$$

$$\varepsilon_1(\lambda) = n(\lambda)^2 - k(\lambda)^2 \qquad (18)$$

$$\varepsilon_2(\lambda) = 2n(\lambda)k(\lambda) \qquad (19)$$

The calculated values of $\varepsilon_1(\lambda)$ and $\varepsilon_2(\lambda)$ are presented in figures 11, 12 respectively. From this study, ε_∞, ω_p, and τ, which are respectively high frequency dielectric constant, plasma frequency and relaxation time, through the relations:

$$\varepsilon_1 \approx \varepsilon_\infty - \frac{\varepsilon_\infty \omega_p^2}{4\pi^2 c^2}\lambda^2 \quad (20)$$

$$\varepsilon_2 = 2nk \approx \frac{\varepsilon_\infty \omega_p^2}{8\pi^3 c^3 \tau}\lambda^3 \quad (21)$$

$$\omega_p^2 = \frac{4\pi N e^2}{\varepsilon_\infty m_e^*} \quad (22)$$

Where N/m_e^* represents free carriers' concentration-to-effective mass ratio. Calculated values of high frequency dielectric constant, plasma pulsation and relaxation time are gathered in table 12.

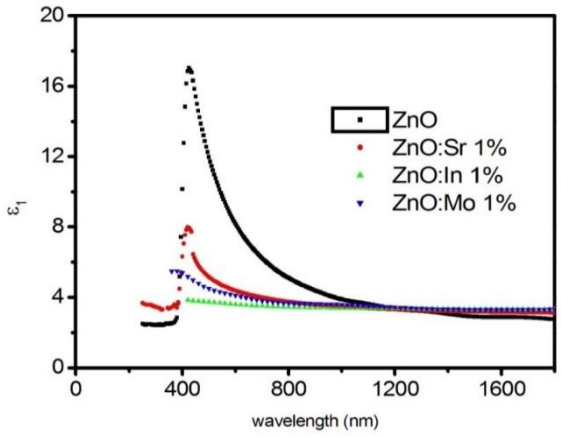

Fig. 11: Variation of the real part of complex dielectric constant with wavelength.

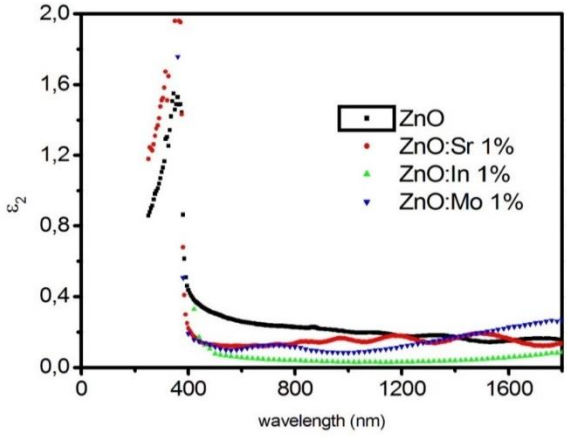

Fig. 12: Variation of imaginary part of complex dielectric constant with wavelength.

Table 12: Values of the dielectric parameters deduced from optical measurements.

	ε_∞	ω_p (10^{14} rds^{-1})	τ (10^{-13} s)
ZnO	3.53	17.3	3.26
ZnO :Sr 1%	3.33	8.66	0.276
ZnO :In 1%	3.42	2.40	8.09
ZnO :Mo 4%	3.41	2.26	6.41

5. Conclusion

In this work, hexagonal zinc oxide (ZnO) thin films doped with Sr/In/Mo were prepared by spray pyrolysis on a glass substrate at 450 °C. The effect of these films on the structural, morphological, optical, and electrical properties was systematically studied. X-ray diffraction (XRD) studies revealed that the films are polycrystalline, with preferred growth along the (002) plane. The optical band gap was found to be in the range of 3.219–3.297 eV. Urbach energy estimation indicates that the resulting optical band gap is subject to disorder changes in the Sr/In/Mo-doped ZnO films. The real (n) and imaginary (k) parts of the complex refractive index were determined and examined from the dielectric constant of these prepared thin films. The dispersion of the films was studied using both the Cauchy model and the Wimble-Di-Domenico

method. The Cauchy coefficients A and B, as well as the oscillator energy E0 and the scattering energy Ed, were calculated. The films were found to have vertical scattering over the entire wavelength range, with the oscillator energy E0 and scattering energy Ed reaching a maximum of about 15 eV at low doping levels. The optical coefficients were also calculated. Finally, in agreement with the analyses of the transmittance derivatives, elements of the lattice conformal theory were proposed as a possible explanation for the preferred incorporation of indium within the ZnO würtzite lattice, compared to the incorporation of molybdenum and strontium. Further studies are underway to determine the electrical properties, conductivity mechanisms, and magnetic properties of these doped films.

References

1. B. Jun, S. Lee, GL. Messing, Key Engineering Materials 317-318, (2006) 207.
2. B. Ouni, M. Haj Lakhdar, R. Boughalmi, T. Larbi, A. Boukhachem, A. Madani, K. Boubaker, M. Amlouk, Journal of Non-Crystalline Solids, 367 (2013) 1.
3. R. Boughalmi, A. Boukhachem, M. Amlouk, Materials Science in Semiconductor Processing, 30 (2015) 218.
4. A. Bouzidi, N. Ben ramdane, H. Tabet-Derraz, C. Mathieu, B. Khelifa, R. Desfeux, Mater Sci Eng B 97 (2003) 5.
5. W. J. Tseng, J. Chang, Ceramics International, 40 (2014) 16779-16784.
6. J. S. Lee, H. S. Kim, J. S. Lee, N. Park, T. J. Lee, M. Kang, Ceramics International, 38 (2012) 6685-6691.
7. L. Zhu, Q. Huang, W. Liu, Ceramics International, 34 (2008) 1729-1733.
8. T. Kohara, H. Tamagaki, Y. Ikari, H. Fujii, Surface & Coatings Technology 185 (2004) 166.
9. O. Zywitzki, G. Hoetzsch, urf. Coat. Technol. 86/87 (1996), 640-647.
10. V.N Jmerik, V.V Mamutin, T.V Shubina, M.G Tkachman, V.A Vekshin, V.V Ratnikov, A.V Lebedev, S.V Ivanov, P.S Kopèv, Proceedings of the 8th International Symposium Nanostructures: Physics and Technology, 2000, Pages 125.
11. H.M. Martínez, J. Torres, L.D. López Carreño, M.E. Rodríguez-García, Material characterization 75 (2013)184.
12. M. Halvarsson, V. Langer, S. Vuorinen, Surface and Coatings Technology 76-77(1995) 358.
13. A. Boukhachem, B Ouni, M Karyaoui, AMadani, R Chtourou, M Amlouk, Mater. Sci. Semicond. Process. 15 (2012) 282.
14. M. Ristova, Y. Kuo, S. Lee, Semiconductor Science and Technology 18 (2003) 788.
15. X.Y. Li, H.J. Li, Z.J. Wang, H. Xia, Z.Y. Xiong, J.X. Wang, Optics Communications 282 (2009) 247.
16. R. Tripathi, A. Kumar, C. Bharti, T. P. Sinha, Current App. Phys.10 (2010) 676.
17. W. Jang, Y. Lu, W. Hwang, T. Hsiung, H.P. Wang, Surface and Coatings Technology.202 (2008) 5444.
18. P. P. Sahay, R.K. Nath, Sensors and Actuators B: Chemical 2 (2008) 654.
19. M.A. Mahdi, Z. Hassan, S.S. Ng, J.J. Hassan, S.K. Mohd Bakhori, Thin Solid Films 520 (2012) 3477.

20. Qasem A. Drmosh, Saleem G. Rao, Zain H.Yamani, Mohammed A. Gondal,"Crystalline nanstructured Cu doped ZnO thin films grown at room temperature by pulsed laser deposition and their characterization",Appl. Surf. Sci.,vol.270, pp.104–108, Mar 2013.
21. J. Ramesh, G. Pasupathi, R. Mariappan, V. Senthil Kumar, V. Ponnuswamy, "Structural and optical properties of Ni doped ZnO thin films using sol-gel dip coating technique",Optik, vol.124, pp.2023– 2027, Aug 2013.
22. Hua Zhu, Hemei Wang, Wenqiong Wan, Shijin Yu, Xiao Wei Feng,"Influence of oxygen and argon flow on properties of aluminum doped zinc oxide thin films prepared by magnetron sputtering", Thin Solid Films,vol.566, pp. 32–37, Sept 2014.
23. A. Yamada, B. Sang, M. Konagai. "Atomic layer deposition of ZnO transparent conducting oxides". Appl. Sur. Sci. V112, Marsh 1997, 216-222.
24. R. Müller**,** F. Huber, O.Gelme, M. Madel, JP. Scholz, A. Minkow, U.Herr and K. Thonke. " Chemical Vapor Deposition Growth of Zinc Oxide on Sapphire with Methane: Initial Crystal Formation Process". Crystal Growth & Design, Vol 19/Issue 9, July 16, 2019.
25. A. Souissi, A. Boukhachem, Y. Ben Taher, A. Ayadi, A. Mefteh, M. Ouesleti,S. Guermazia, M. Amlouk,"Structural and vibrational studies of Mo and In doped ZnO sprayed thin films",Optik,vol.125, pp.3344–3349, 2014.
26. A. Jagannatha Reddy, M. K. Kokila, H. Nagabhushana, S.C. Sharma, J.L. Rao, C. Shivakumara, B.M. Nagabhushana, R.P.S. Chakradhar, Materials Chemistry and Physics 133(2012) 876.
27. Y. Narendar, G. L. Messing, Catal. Today, 35 (1997) 247.
28. K. Boubaker, Materials Science and Engineering A, 528 (2011) 1455.
29. A. Boukhachem, C. Bouzidi, R. Boughalmi, R. Ouerteni, M. Kahlaoui, B.Ouni, H. Elhouichet, M. Amlouk, Ceramics International, 40(2014) 13427.
30. M.P. Dare-Edwards, A.H. Goodenough, A. Hammett, P.R. Trevellick, Faraday Trans., 179 (1983) 2027.
31. D. Barreca, C. Massignan, S. Daolio, M. Fabrizio, C. Piccirillo, L. Armelao, E. Tondello, Chem. Mater., 13 (2001) 588.
32. F. Urbach, Phys. Rev. 92 (1953) 1324.
33. W. Martienssen, J. Phys. Chem. Solids, 2 (1957) 257.
34. A. Boukhachema, S. Fridjine, A. Amlouk, K. Boubaker, M. Bouhafs, M. Amlouk, J. of Alloys and Compounds 501 (2010) 339.
35. A. Amlouk, K. Boubaker, M. Amlouk, J. Alloys Compd., 490 (2010) 602.
36. R.D. Shannon, Acta Crystallographica Section A: Crystal Physics, Diffraction, Theoretical and General Crystallography 32 (1976)751-767.
37. M. Ben Amor, A. Boukhachem, K. Boubaker, M. Amlouk, Materials Science in Semiconductor Processing, 27 (2014) 994.
38. R. Boughalmi, A. Boukhachem, M. Kahlaoui, H. Maghraoui, M. Amlouk, Materials Science in Semiconductor Processing, 26 (2014) 593.
39. R. Boughalmi, A. Boukhachem, I. Gaied, K. Boubaker, M. Bouhafs, M. Amlouk, Materials Science in Semiconductor Processing, 16 (2013) 1584.
40. A. Ramirez-Duverger, A. Rabdel Ruiz-Salvador, M.P. Hernandez-Sanchez, M.F. Garcia-Sanchezd, G. Rodriguez-Gattornod, Solid State Ionics, 96 (1997) 89.
41. A. K. Jonscher, The 'Universal' Dielectric Response, Nature, 267 (1977) 673.

42. M. Di-Domenico, M. Eibschütz, H.J. Guggenheim, I. Camlibel, Solid-State Communications, 16 (1969) 1119.
43. C. A. Arguello, D. L. Rousseau and S. P. S. Porto, Phys Rev, 181 (1969) 13511363
44. M. L. Glasser, J. Phys. Chem. Solids, 10 (1959) 229-233.
45. T. C. Damen, S. P. S. Porto, B. Tell, Phys. Rev. 142, 570 (1966).
46. A. Boukhachem, C. Bouzidi, R. Boughalmi, R. Ouerteni, M. Kahlaoui, B. Ouni, H. Elhouichet, M. Amlouk, Ceram. Int. 0 (2014) 13427.
47. W. Cao, R. Gerhardt, Solid State Ionics 42 (1990) 213.
48. B. Ouni, A. Boukhachem, S. Dabbous, A. Amlouk, K. Boubaker, M. Amlouk, Materials Science in Semiconductor Processing, 13 (2010) 281.
49. A. K. Wolaton, T. S. Moss, Proceedings of the Royal Society A, 81, (1963) 5091.
50. M. Sesha Reddy, K.T. Ramakrishna Reddy, B.S. Naidu, P.J. Reddy, Optical Materials, 4 (1995) 787.
51. M. Karyaoui, A. Mhamdi, H. Kaouach, A. Labidi, A. Boukhachem, K. Boubaker, M. Amlouk, R. Chtourou, Materials Science in Semiconductor Processing, 30(2015)255.
52. N. F. Mott, Nobel Prize Lecture (1977).
53. B. Ouni, M. Haj Lakhdar, R. Boughalmi, T. Larbi, A. Boukhachem, A. Madani, K. Boubaker, M. Amlouk, J. of Non-Crystalline Solids 367 (2013) 1.
54. A. Boukhachem, A. Yumak S. Krichen, A. Madani, M. Abderrabba, P. Petkova, K. Boubaker, M. Amlouk, H. Bouchriha, Sensors and Actuators A 227 (2015) 11.
55. K. Boubaker, Journal of Ceramics, 2013 (2013) 6.
56. K. Boubaker, M. Amlouk, Y. Louartassi, H. Labiadh, J. Aust. Ceram. Soc., 49 (2013)109.
57. K. Ben Messaoud, A. Gantassi, H. Essaidi, J. Ouerfelli, A. Colantoni, K. Boubaker, M. Amlouk, Adv. in Mater. Sci. and Engin. 2014 (2014) 1.
58. R. Mimouni, K. Boubaker, M. Amlouk, J. of Alloys and Compounds, 624 (2015) 189.
59. S. Belgacem, R. Benameur, Rev. Phys. Appl. 25 (1990)1245.
60. S. R. Bathe, P.S. Patil, Sol. Energy Mater. Sol. Cells 91(2007)1097.
61. G.E. Pike, A.C. conductivity of scandium oxide and a new hopping model for conductivity, Physical Review B 6 (1972) 1572.
62. P. Hansson, M. Halvarsson, S. Vuorinen, Surface and Coatings Technology 76-77 (1995) 256.
63. B. Roy, S. Chakrabarty, O. Mondal, M. Pal, A. Dutta, Mater. Char. act., 70 (2012) 1.
64. S. H. Wemple, Solid-State Communications, 12 (1973) 701.